Journal of Colloid and Interface Science 473 (2016) 1–8

Contents lists available at ScienceDirect

Journal of Colloid and Interface Science

journal homepage: www.elsevier.com/locate/jcis

Calcium hydroxide nanoparticles from solvothermal reaction for the deacidification of degraded waterlogged wood

Giovanna Poggi [a], Nicola Toccafondi [a], David Chelazzi [a], Patrizia Canton [b], Rodorico Giorgi [a], Piero Baglioni [a,*]

[a] Department of Chemistry & CSGI, University of Florence, Via della Lastruccia 3, 50019 Sesto Fiorentino, Florence, Italy
[b] Department of Physical Chemistry and CSGI, University of Venice Ca' Foscari, 30170 Venezia, Italy

GRAPHICAL ABSTRACT

ARTICLE INFO

Article history:
Received 1 February 2016
Revised 15 March 2016
Accepted 17 March 2016
Available online 18 March 2016

Keywords:
Deacidification
Wood
Vasa
Calcium hydroxide nanoparticles
pH-adjustment
Cellulose

ABSTRACT

Hypothesis: A combination of acid and iron ions inside the wood has been corroding the cellulose matrix of the Swedish warship Vasa, imposing its deacidification. Past deacidification treatments displayed poor penetration inside the wood matrix with limited efficacy. A vacuum assisted treatment of wood using newly developed calcium hydroxide nanoparticle dispersions represents a possible candidate for the treatment of acidic waterlogged wood objects such as sculptures and decorative artifacts.
Experiments: A solvothermal process was used for the synthesis of calcium hydroxide nanoparticle dispersions. Before the application on waterlogged wood, the physico-chemical characterization of these systems was carried out using several techniques. The efficacy of the deacidification treatment of wood samples from the Vasa was assessed by determination of pH and Differential Thermal Gravimetric (DTG) measurements.
Findings: The proposed solvothermal reactions can be used to produce stable and highly concentrated calcium hydroxide nanoparticle dispersions in alcohols, needing no further purification before the application. This process has also the advantage to be upscalable to industrial level. Both pH and DTG measurements showed that the newly developed dispersions can homogenously penetrate inside the wood up to 20 cm, neutralizing acidity and creating an alkaline buffer inside the wooden matrix, to hinder the degradation of residual cellulose.

* Corresponding author.
E-mail addresses: poggi@csgi.unifi.it (G. Poggi), toccafondi@csgi.unifi.it (N. Toccafondi), chelazzi@csgi.unifi.it (D. Chelazzi), cantonpa@unive.it (P. Canton), giorgi@csgi.unifi.it (R. Giorgi), piero.baglioni@unifi.it (P. Baglioni).

http://dx.doi.org/10.1016/j.jcis.2016.03.038
0021-9797/

1. Introduction

In 1628, on the day of its maiden voyage, the Vasa sunk into the brackish and polluted water of the Stockholm harbor, from which it was recovered more than 300 years later. In order to prevent the shrinkage of the wet wooden structure, PEG aqueous solutions were sprayed on the shipwreck for 17 years. Nowadays, the preservation of the Vasa is threatened by the concomitant action of acid-catalyzed hydrolysis and metal-catalyzed oxidation (Fenton reactions). Acidic compounds include sulfuric acid, mainly present in the upper layers, and organic acids, such as oxalic acid, whose concentration increases with depth. Oxidative degradation is promoted by iron salts present inside the wood [1–7]. For the extraction of iron ions the usage of aqueous solutions of chelating agents (e.g. ethylenediimino-bis(2-hydroxy-4-methylphenyl) acetic acid, EDDHMA) has been proposed and tested [8], but the preservation of the Swedish warship Vasa is still a challenge for wood conservators. The Vasa is indeed a unique conservation challenge, but there are several other waterlogged ships and objects, such as, for instance, the English carrack-type warship Mary Rose or the Norwegian Oseberg burial finds, whose preservation is threatened by acidity and oxidation.

Hydrolysis and oxidation are the two main degradation processes that affect cellulose-based works of art. Since hydrolysis and oxidation usually act in a synergistic way by creating the so-called *spiraling effect* [9], both a deacidification intervention and an antioxidant treatment should be applied. Several groups have indeed proposed antioxidant materials to be combined with the commonly used deacidification treatments [10–14]. Recently we proposed a new method, based on the use of nanoparticles of calcium or magnesium hydroxide [15,16], able to stop cellulose degradation mechanisms induced by metal ions and acidity. The method takes advantage from the much slower pace of the catalytic activity of metal ions around neutrality [17]. Conservation of cellulose can be achieved in a single-step pH-controlled deacidification treatment to inhibit the acid-catalyzed hydrolysis and the metal-catalyzed oxidation, prolonging the useful life of the artifacts.

Calcium hydroxide nanoparticles, obtained from homogeneous-phase reactions, were originally designed for the consolidation of wall paintings [18], and subsequently used for the deacidification of cellulosic materials, i.e., paper, canvas, wood [19–25]. However, the required purification and the small amount of particles obtained from the homogeneous-phase pathway made this procedure time-consuming. Preparation pathways based on the grinding and dispersion of slaked lime have been also considered as potentially rapid and simple ways to obtain high amounts of particles [26,27]. The size of particles obtained with this method is in the range from 300 nm to 700–800 nm, which can result in limited penetration when the porosity of the substrates is lowered by the presence of protective coatings or consolidants. An improvement was achieved using a thermo-mechanical treatment for hydration of calcium oxide [26,27], but the need of highly reproducible particles' size distributions led to the development of different strategies. In particular, a bottom-up synthetic procedure for the "scaling down" of particles size is presented here, and the obtained particles penetrate more homogenously through low porous materials, i.e. PEG-consolidated archeological wood.

Calcium hydroxide nanoparticles were synthesized starting from metallic calcium and short-chain alcohols, i.e., ethanol, and *n*-propanol. At high temperature and pressure, calcium alkoxide is formed; the subsequent hydrolysis of this compound yields nanoparticles of calcium hydroxide already dispersed in the appropriate solvent, and the system can thus be directly applied for conservation purposes because no purification step is needed. It is worth noting that the usage of non-aqueous medium for the synthesis hinders the growth of nanoparticles due to Ostwald ripening [28–32]. Besides the decreased particles' dimensions, the advantage of this new synthetic procedure, based on the widely used solvothermal process for oxide nanoparticles syntheses [33–35], relies in the feasible upscale of the process to industrial level, with great benefits in terms of costs.

Calcium hydroxide nanoparticle dispersions obtained from the solvothermal reactions were characterized by Attenuated Total Reflectance Fourier Transform Infrared Spectroscopy (ATR-FTIR), X-ray Powder Diffraction (XRPD), High Resolution Transmission Electron Microscopy (HR-TEM), Selected Area Electron Diffraction (SAED), Dynamic Light Scattering (DLS), surface area analysis, and turbidimetry measurements, before being applied to hardwood samples from the Vasa warship. The efficacy of the deacidification treatment was assessed by determination of pH and Differential Thermal Gravimetric (DTG) measurements.

2. Materials and methods

2.1. Chemicals

Ethanol absolute (99.8%, Fluka), *n*-propanol (99.5%, Sigma-Aldrich), and metal granular calcium (99%, Aldrich) were used for nanoparticle syntheses. Highly pure water (resistivity >18 MΩ cm, by a Millipore Milli-Q UV system) was used.

2.2. Nanoparticles synthesis

The hydroxide nanoparticle syntheses were performed in a high-pressure reactor (Parr-instruments) by a one-pot reaction consisting of two steps:

$$\mathrm{Ca} + \mathrm{Alcohol} \rightarrow \mathrm{Ca(alkoxide)_2} + \mathrm{H_2} \quad (1)$$

$$\mathrm{Ca(alkoxide)_2} + \mathrm{H_2O} \rightarrow \mathrm{Ca(OH)_2} + \mathrm{Alcohol} \quad (2)$$

During the first step of the reaction, the alcohol (ethanol or *n*-propanol) oxidizes metal calcium to the corresponding alkoxide (1). The subsequent addition of water induces the formation of calcium hydroxide via a hydrolysis reaction (2).

In particular, 10 g of granular calcium and 500 mL of alcohol (ethanol or 1-propanol) were placed inside a high-pressure reactor. Before starting the reaction, vacuum/nitrogen cycles were performed to ensure an oxygen-free atmosphere inside the sealed reaction chamber. During the reaction, an increase in pressure due to both solvent evaporation and hydrogen release was observed. In order to hydrolyze the alkoxide to calcium hydroxide, 35 mL of water was added inside the reaction chamber by means of steel pipette in a nitrogen atmosphere. Water addition was carried out at 70 °C for 60 min, regardless of the alkoxide nature. In Table 1 the reaction temperatures are indicated.

Table 1
Relative permittivity, solvent acidity (SA) and temperature used for the alkoxide formation and the alkoxide hydrolysis.

Alcohol	System name	Relative permittivity	SA	Alkoxide synthesis (°C)	Alkoxide hydrolysis (°C)
Ethanol	E	24.5	0.4	65	70
n-Propanol	1P	20	0.367	130	70

2.3. Nanoparticles characterization

Dynamic Light Scattering (DLS) measurements were performed with a 90Plus Particle Size Analyzer (Brookhaven Instrument Corporation). The light scattered from the sample was collected at 90° with the incident 659 nm laser light radiation. The measurements were recorded at 25 °C. Particle size distributions were obtained from the fitting of the measured autocorrelation functions using the CONTIN method [36]. Each sample was diluted to 1 g/L before the measurement.

Transmission Electron Microscopy (TEM) was performed using a JEOL JEM3010 operating at a 300 kV acceleration voltage, point to point resolution 0.17 nm at Scherzer defocus. For the preparation of TEM samples, each dispersion was diluted to 0.25 g/L, that is an appropriate concentration to obtain systems homogenously distributed on a holey carbon Cu-grid. The images were analyzed by the ImageJ routine as described by Pyrz and Buttrey [37]. Ellipses with a cut off area set at 50 nm^2 were used to circumscribe the particles and their major axis values were plotted as a function of counts.

The chemical composition of the obtained particles was determined by ATR measurements, carried out with a Thermo Nicolet Nexus 870 spectrometer equipped with a liquid nitrogen-cooled Mercury Cadmium Telluride detector and a single reflection diamond crystal ATR unit. The spectra were obtained from 128 scans with 4 cm^{-1} of optical resolution, in the 4000–650 cm^{-1} range.

XRPD patterns were recorded at 25 °C, with a step size of 0.05° in a 2θ scattering angle. A Philips X'Pert system equipped with a focusing graphite monochromator on the diffracted beam and a proportional counter with an electronic pulse height discrimination was used. Moreover, a divergence slit of 0.5°, a receiving slit of 0.2 mm, an antiscatter slit of 0.5°, and Ni-filtered Cu KR radiation (30 mA, 40 kV) were used.

To evaluate the stability of nanoparticle dispersions, turbidimetry measurements were performed with a Varian Cary 100 Bio spectrophotometer, equipped with a Peltier Multi-block; the absorbance of the sample at 600 nm was measured as a function of time. Absorbance was assumed proportional to the system turbidity: the decrease of absorbance over time is due to particles aggregation and settling. Measurements were carried out at 25 °C, using sealed quartz cuvettes with an optical path of 1 cm.

Specific surface area of nanoparticles was measured by N_2 sorption isotherms (BET) using a Coulter SA 3100 Surface area analyzer. This gives access to the value of the surface area with an error of about 5%. From the BET surface area an average particles size can be estimated by calculating the equivalent spherical diameter, or BET particle diameter (d_{BET}), from the equation: $d_{BET} = 6/(\rho \cdot S_w)$, where ρ is the density of calcium hydroxide (2.211 g/cm^3) and S_w is the specific surface area [38]. The particle surface area determined by Brunauer-Emmett-Teller (BET) measurements is about 34 m^2/g for the 1P system and 36 m^2/g for the E system. From this value, a spherical equivalent diameter of 80 nm and 75 nm, respectively, can be calculated [38]. The d_{BET} particles diameter are lower than those obtained from TEM images analysis due to the fact that nanoparticles tend to cluster once dried on the TEM holey carbon Cu-grid.

2.4. Deacidification and characterization of wood samples

Oak wood specimens (20 mm × 20 mm × 80 mm) were obtained from an original Vasa timber (sample number 65517). Before the deacidification treatments, the samples were immersed for 7 days in a continuous flux of demineralized water. The samples were then dried in air at room temperature for a week, before being treated. As shown in the experimental section, this treatment leads only to a partial removal of PEG, preventing the shrinkage of the wood structure. A specific vacuum treatment was designed (Fig. 1) for the deacidification of wood samples. Washed and dried specimens were covered with a sealing film leaving uncovered only 5 mm from the bottom face. From now on the bottom face will be referred to as "0 cm". On top of the sample, a vacuum junction was placed and fastened to the top face with the sealing film. The top face will be referred to as "8 cm". A diaphragm pump, connected to the junction, was used to create a small pressure depression on the 8 cm surface. This facilitates the intake of the deacidifying dispersion where the uncovered portion of the samples was immersed. A 1 mm gap was left between the sealed portion of the wood and the meniscus of the dispersion, to avoid suction of the latter into the interspace between the sealing film and the longitudinal faces.

A deacidification cycle consisted in the suction of 5 mL of dispersion and in a subsequent 24 h drying step. Six cycles were performed for each sample, until a total amount of 30 mL of dispersion was drawn through the oak wood.

After deacidification, possible small white deposits present on "8 cm" were gently removed mechanically with a soft brush. Then, each sample was cut in half, recovering the sawdust (from now on the samples taken from the middle section will be referred to as "4 cm"). Sawdust was also collected from the top and bottom face.

The thermal behavior of wood specimens was studied with a SDT Q600 TA Instrument, operating between 25 and 550 °C at a heating rate of 10 °C/min under nitrogen flow (100 mL/min). For each measurement, ca. 5 mg of sawdust was placed inside an aluminum pan. 125 mg of sawdust, preconditioned at 25 °C and 50% RH for two days in vials, was used for the pH measurements of wood. 9 mL of de-carbonated water was added in each vial, which was subsequently sealed, in order to avoid the solubilization of CO_2 from air. The vials were kept under stirring for 1 h, before measuring the pH of the "extraction" water with a digital pH-meter CrisonBasic 20, equipped with a combined electrode, model 52-21. Measurements on highly inhomogeneous samples like archeological wood are affected by an error of ca. 0.5 pH units.

Further experiments were conducted on larger Vasa wood samples (sample number 65517), measuring 20 mm × 20 mm × 200 mm. For these samples, 80 mL of nanoparticle dispersions was applied using the same experimental procedures described

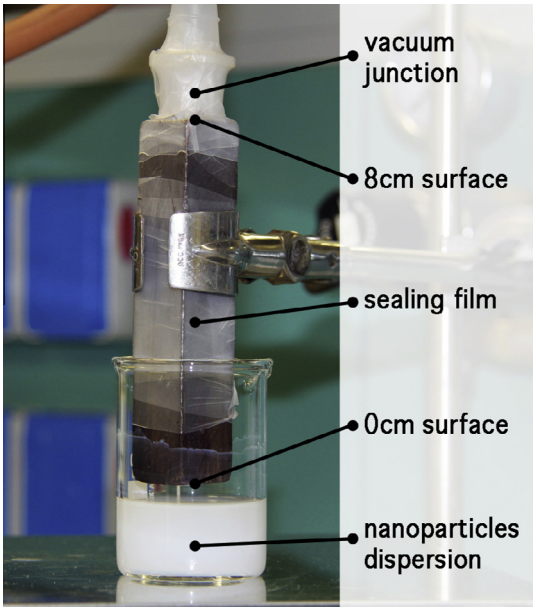

Fig. 1. View of the vacuum treatment of Vasa samples.

above. As previously indicated, wood samples were characterized by pH determinations and DTG measurements.

3. Results and discussion

3.1. Synthesis and characterization of calcium hydroxide nanoparticles

The deacidification treatment of wooden artifacts must fulfill some applicative requirements: (i) the treatment must not induce any changes in the appearance of artifacts; (ii) in order to achieve a highly homogenous treatment, dispersions must be stable for a considerable amount of time, i.e. from several hours up to days; (iii) the final pH of samples should not be excessively basic because, in the presence of oxidized cellulose, high pH values may induce depolymerization due to the β-alkoxy elimination mechanism [39,40].

Solutions of alkaline earth metal alkoxides are nowadays used for deacidification purposes, e.g., the Papersave Process® [41]. In our case, alkoxides were chosen as precursors of calcium hydroxide dispersions, with the purpose of obtaining smaller particles as compared to those previously synthesized by us for the conservation of wall paintings [26].

Ethanol and *n*-propanol, having different reactivity towards the metal, were used. Ethanol has a higher oxidizing capacity [42] as shown in Table 1. The solvent acidities indicated in Table 1 are obtained comparing the solvatochromism of two betaine dyes [43] (o-*tert*-butylstilbazolium betaine dye, TBSB, and o,o′-di-*tert*-butylstilbazolium betaine dye, DTBSB) as suggested by Kamlet and Taft [44]. Relative permittivity and solvent acidity are both related to the solvent reactivity. Therefore, the oxidizing reaction of metal calcium has been performed at 65 °C for ethanol and 130 °C for *n*-propanol. A higher amount of water than the stoichiometric value is required to completely hydrolyze the alkoxide (see Experimental section). In Fig. 2, the IR spectra of E and 1P dried powders are reported. The characteristic peak of calcium hydroxide can be observed at 3640 cm^{-1}. The presence of a weak C=O stretching peak at 1500 cm^{-1}, and bands at 876 cm^{-1} and 713 cm^{-1}, is due to incipient conversion into carbonate of the hydroxide nanoparticles that, due to their high surface area, react readily with atmospheric CO_2. Weak bands at 2830–2960 cm^{-1} (C—H stretching) and around 1075 cm^{-1} (C—O stretching) can be ascribed to alcohol or alkoxide [45].

The size distribution of the calcium hydroxide particles was obtained from DLS measurements (cumulant method) and TEM image analysis. TEM images of system E showed a homogenous distribution of particles over the thin graphite film, even though some clusters of particles are visible (Fig. 3A).

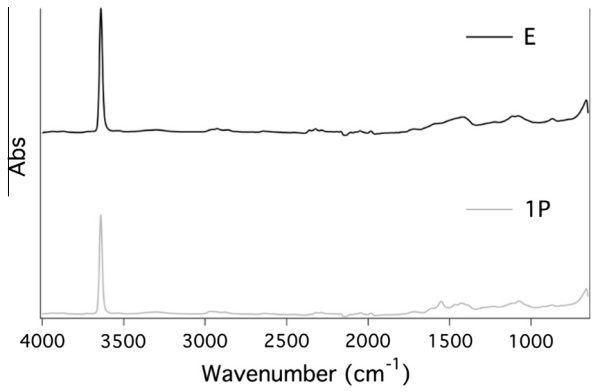

Fig. 2. IR spectra of calcium hydroxide dried powders obtained from the nanoparticle dispersions E and 1P (produced in ethanol and *n*-propanol respectively).

The mean hydrodynamic diameter of E system particles, obtained by DLS measurements, is 206 nm (see Fig. S1A), whereas the size distribution obtained from image analysis (TEM) is centered at 170 nm (Fig. 3B).

Selected Area Electron Diffraction (SAED) analysis performed on a single hexagonal nanoparticle (Fig. 3C and D) confirms the presence of calcium hydroxide: the experimental lattice parameters are in good accordance with the reference values of Portlandite, i.e. the crystalline form of calcium hydroxide (see Table S2).

XRPD measurements of system E confirmed that the reaction product is composed of highly crystalline particles of Portlandite (see Fig. 4), supporting that calcium hydroxide nanoparticles obtained from the proposed synthesis can be safely used on works of art without further purification.

During the drying step required by TEM sample preparation, 1P system nanoparticles clustered, as can be seen from the electron microscopy images (Fig. 5A). Despite the fact that this behavior makes the dimensional analysis of particles difficult, after a meticulous preliminary elaboration of the images [37], accurate size distributions were obtained. Analysis of the TEM revealed a mean particle diameter of 180 nm (Fig. 5B). The CONTIN fitting of system 1P showed a monomodal distribution of particles size centered at 239 nm (see Fig. S1B). SAED analysis performed on a particles cluster (black square in Fig. 5A), displays the typical pattern of calcium hydroxide lattice: in particular, reflexes from the reciprocal lattice planes (1 0 0) and (1 0 1) corresponding to 3.10 Å and 2.61 Å lattice distances are present (Fig. 5C).

It is interesting to note that the synthesized nanoparticles are polycrystalline, meaning that differently orientated calcium hydroxide crystallites can be found, as shown in the HR-TEM picture (Fig. 5D).

As for the E system, XRDP showed that calcium *n*-propoxide was hydrolyzed into hydroxide (see Fig. 4).

The kinetic stability of the synthesized calcium hydroxide dispersions was evaluated before proceeding to the application. The kinetic stability of E and 1P dispersions is particularly high. The normalized absorbance at 600 nm, monitored for 6 h, showed that no settling of $Ca(OH)_2$ nanoparticles occurred (Fig. S3). Visual inspection showed that the particles dispersions are stable even after months from preparation. Therefore, both dispersions are eligible for practical application onto works of art.

Overall, the physico-chemical characterization of E and 1P systems showed that the solvothermal reaction presented in this paper yields stable and highly concentrated (35 g/L) nanoparticle dispersions that do not require any purification step before the application. The time required for the synthesis and the amount of produced particles, are both critical aspects in the case of the treatment of large objects, i.e., statues and decorative artifacts from the Vasa. The solvothermal process allows for a significant decrease in terms of costs with respect with the state-of-the-art synthetic routes for the preparation of alkaline nanoparticles for deacidification.

3.2. Deacidification of wood samples from Vasa

In order to evaluate the deacidification efficacy of the synthesized dispersions E and 1P, pH determinations and DTG measurements were carried out on wood samples. For each pH determination, 125 mg of sawdust is required, which is a significantly high amount of sample as far as artistic objects are concerned. On the other hand, the use of thermogravimetry for characterizing archeological and historical wood is advantageous because it provides reliable results and only few milligrams of sample are needed for a single thermal measurement. The pyrolysis temperature of cellulose (T_p), that is the temperature at which the weight loss derivative is maximum, can be considered as an

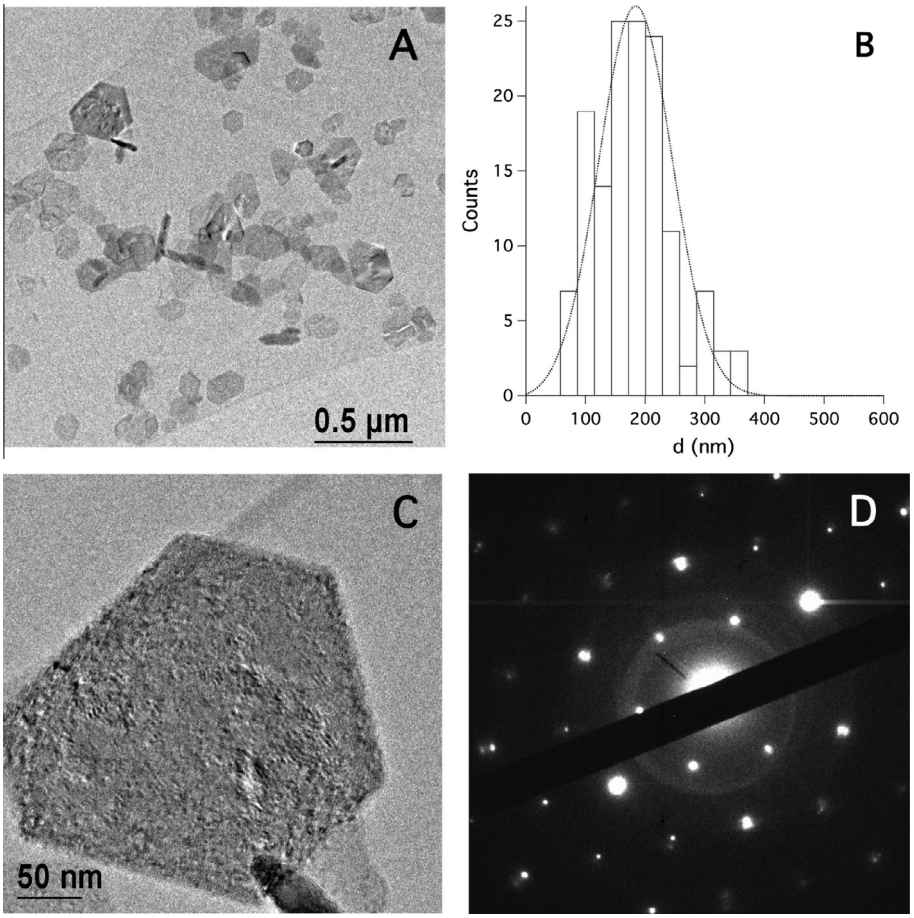

Fig. 3. (A) TEM image of system E nanoparticles (8k nominal magnification). (B) Size distribution of system E nanoparticles obtained from TEM images analysis. (C) TEM image of a system E nanoparticle (50k nominal magnification). (D) Selected Area Electron Diffraction (SAED) analysis conducted on (C).

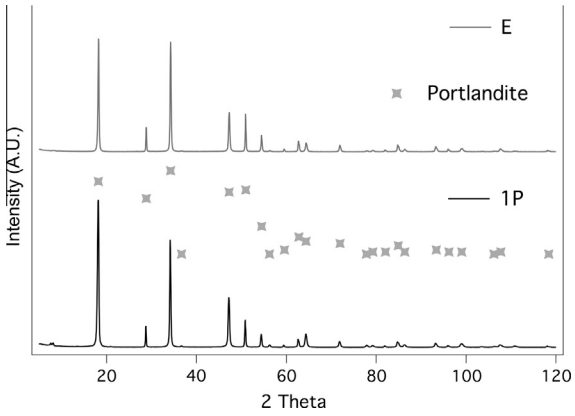

Fig. 4. Comparison between XRPD spectra of system E and 1P powders. Stars label the Portlandite peaks used as a reference [46].

indicator of the conservation status of the wood. The thermal behavior of cellulose is strictly related to its chemical environment: the dehydration of cellulose, that is the first step of the thermal degradation, is promoted and accelerated by acidity [47]. In previous studies, we have shown that after a deacidification treatment the thermal behavior of cellulose changes, and higher values of the pyrolysis temperature are associated to a better conservation state of cellulose [20,22].

In Fig. 6, a comparison between Vasa samples before and after the washing treatment (Untreated and Washed) is reported: the peak ascribed to cellulose pyrolysis (T_p) can be seen at about 330 °C, whereas that due to the thermal degradation of PEG is found at higher temperature. In fact, depending on the M_w of the pristine polymer (or on the average M_w when mixed solutions of PEG were applied), the pyrolysis temperature of polyethylene glycol ranges between 370 °C and 420 °C [48,49]. After the washing treatment, the decrease in the area of the PEG peak is due to partial removal of the PEG oligomer. Cellulose T_p slightly increased after the washing treatment (see Fig. 7), in agreement with the partial removal of acidic compounds, such as oxalic acid produced by the oxidation of cellulose and formic acid formed by the degradation of PEG (induced by the combined action of iron ions and acidity) [5]. It is worth noting that a slight increase in wood pH after washing (about 0.4 unit) was measured regardless of the depth. This increase, even if close to the experimental error, seems to confirm the DTG data.

During water immersion, PEG is solubilized starting from the surface. A seven-day immersion in flowing water ensured partial removal of the consolidant. As it is shown below, the water treatment did not cause shrinkage of the wooden structure upon drying owing to the presence of remaining PEG. Nonetheless, the partial removal of PEG granted good penetration of the particles dispersion.

Both the nanoparticle dispersions in ethanol and *n*-propanol were applied at 5 g/L concentration for the deacidification of Vasa wood sample using the mild vacuum treatment described above.

Characterization of treated wood was carried out at different depths, i.e. at 0 cm, 4 cm and 8 cm from the bottom surface (where the dispersion was suctioned), in order to obtain information about the penetration of particles and deacidification efficacy.

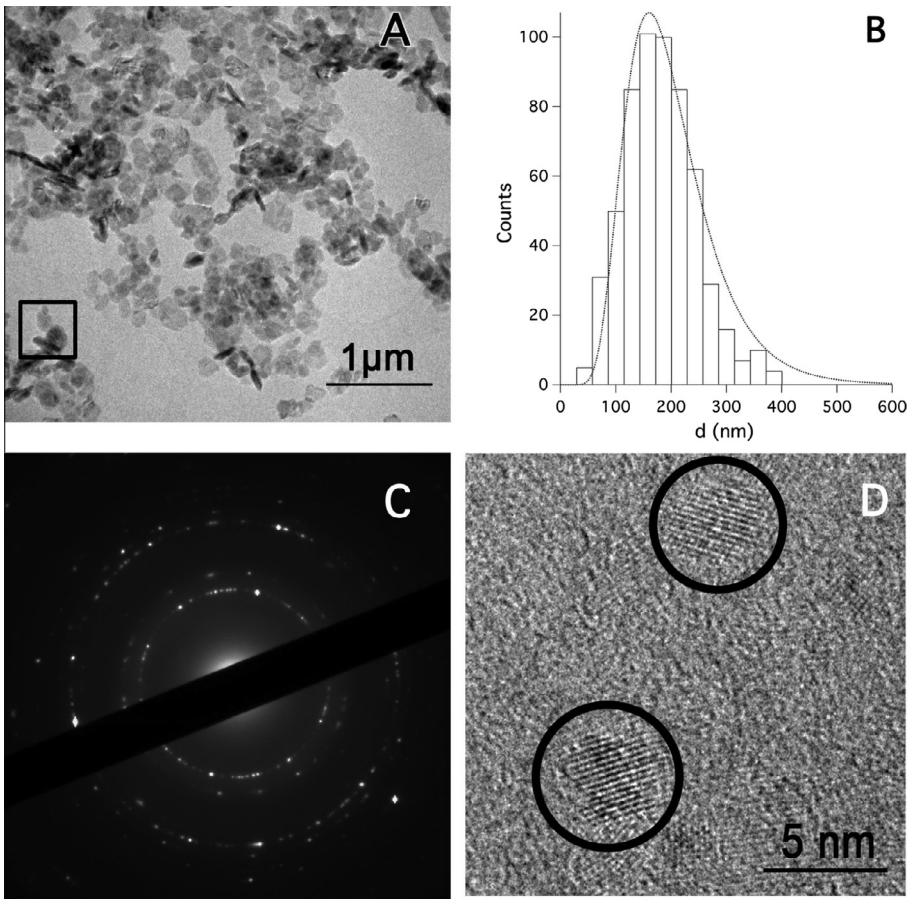

Fig. 5. (A) TEM image of system 1P nanoparticles (4k nominal magnification). (B) Size distribution of system 1P nanoparticles obtained from TEM images analysis. (C) SAED analysis conducted on a nanoparticles cluster (system 1P, black square in Fig. 6A). (D) HR-TEM image (800k nominal magnification) of a single particle of the 1P system, in which polycrystalline structures of 3–4 nm are visible.

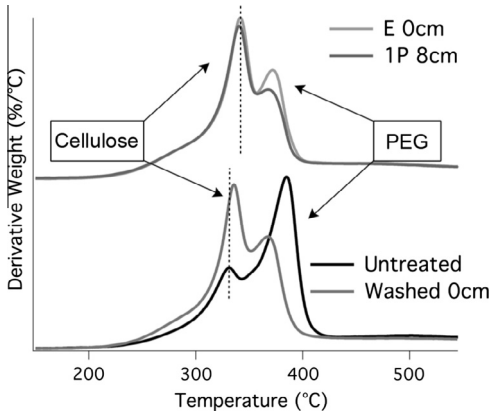

Fig. 6. Comparison between of DTG curves of untreated, washed and deacidified Vasa samples (E 0 cm and 1P 8 cm). The dotted lines help the comparison between cellulose T_p before and after the deacidification treatment.

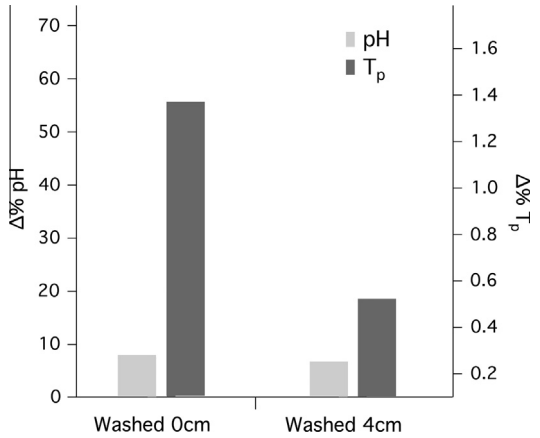

Fig. 7. pH and T_p of washed samples expressed in terms of percentage variation as compared to untreated samples.

For what concerns the specimen treated with the E system, pH and DTG values are in good accordance, regardless of the depth (Fig. 8). It is worth noting that the pH values at 0 cm and 8 cm are very similar, indicating that removal of PEG was sufficient for letting the dispersion flow through the wood and efficiently neutralize acidity. This is also clearly shown by the comparison between the thermograms of deacidified samples reported in Fig. 6. Higher pH variations correspond to significant increases in T_p, confirming that the neutralization of acidity improves the thermal resistance of archeological wood (Fig. 8).

The same good deacidification efficiency was shown by the 1P dispersion. At a depth of 4 cm, a pH close to neutrality was reached, whereas, on both the extremities (0 cm and 8 cm) a pH around 8 was measured. These values are suitable for granting the long-term preservation of the cellulose-based structure. The good accordance between pH and T_p values (Fig. 8) demonstrates that

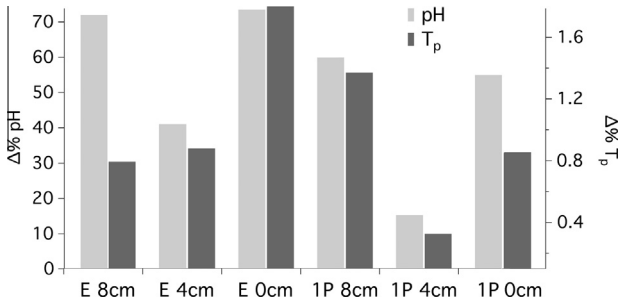

Fig. 8. pH and T_p of deacidified samples expressed in terms of percentage variation as compared to washed samples.

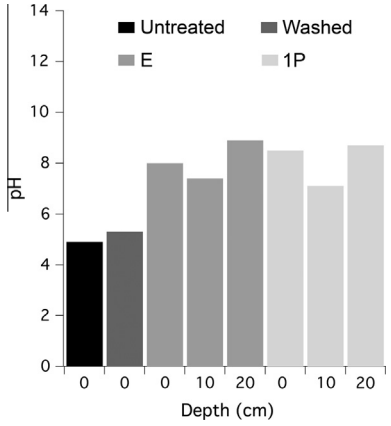

Fig. 9. pH values as a function of depth measured for 20 cm-long Vasa samples. Untreated and washed pH values are also reported for comparison.

the stabilization of pH around neutrality is crucial for improving the conservation status of cellulose.

From the same original Vasa timber, larger samples (20 mm × 20 mm × 200 mm) were obtained and subjected to the same washing and deacidification treatments described above. For these samples, pH values above neutrality were measured regardless of the depth, as reported in Fig. 9.

4. Conclusions

The major limitation in past deacidification treatments of archeological wood relied in the poor penetration of the deacidification systems [20,21,50,51] or, in case of alkaline solutions, in the low amount of deacidification agent that could be uploaded into the wood [52]. A mild vacuum assisted treatment of wood using newly developed pure and highly crystalline calcium hydroxide nanoparticle dispersions was tested. Both pH and DTG measurements on Vasa waterlogged wood showed that dispersions can homogenously penetrate inside the wood up to 20 cm, neutralizing acidity and creating an alkaline buffer inside the wooden matrix to hinder the degradation of residual cellulose and prevent the loss of mechanical properties of the wood. The proposed synthetic pathway yields highly concentrated dispersions of nanoparticles in alcohol needing no further purification before the application, which is a critical aspect for practical applications. The up-scalability of preservation methods is rarely considered in Conservation Science, even though it is a fundamental factor. In our opinion, the mild vacuum assisted treatment coupled with the newly developed nanoparticle dispersions obtained by a solvothermal method is a feasible application methodology and, hopefully, it will be used for the deacidification of large acidic waterlogged wood objects, i.e., statues and decorative artifacts from the warship Vasa.

Acknowledgment

The authors would like to thank Ingrid Hall-Roth and Emma Hocker (from Vasa Museum) for providing wood samples from Vasa and Lars Ivar Elding (University of Lund) for helpful and stimulating discussions. Thanks are also due to Maurizio Ferretti and Alessandro Toccafondi for the preparation of Vasa wood sample (woodcutting). CSGI and European Union (project NANOFORART, FP7-ENV-NMP-2011/282816) is gratefully acknowledged for partial financial support.

Appendix A. Supplementary material

Supplementary data associated with this article can be found, in the online version, at http://dx.doi.org/10.1016/j.jcis.2016.03.038.

References

[1] S. Norbakhsh, I. Bjurhager, G. Almkvist, Impact of iron(II) and oxygen on degradation of oak – modeling of the Vasa wood, Holzforschung 68 (2014).
[2] I. Bjurhager, H. Halonen, E.-L. Lindfors, T. Iversen, G. Almkvist, E.K. Gamstedt, et al., State of degradation in archeological oak from the 17th century Vasa ship: substantial strength loss correlates with reduction in (holo)cellulose molecular weight, Biomacromolecules 13 (2012) 2521–2527.
[3] G. Almkvist, I. Persson, Fenton-induced degradation of polyethylene glycol and oak holocellulose. A model experiment in comparison to changes observed in conserved waterlogged wood, Holzforschung 62 (2008) 704–708.
[4] G. Almkvist, I. Persson, Analysis of acids and degradation products related to iron and sulfur in the Swedish warship *Vasa*, Holzforschung 62 (2008) 694–703.
[5] G. Almkvist, I. Persson, Degradation of polyethylene glycol and hemicellulose in the *Vasa*, Holzforschung 62 (2008) 64–70.
[6] J. Glastrup, Y. Shashoua, H. Egsgaard, M.N. Mortensen, Degradation of PEG in the warship Vasa, Macromol. Symp. 238 (2006) 22–29.
[7] Y. Fors, M. Sandström, Sulfur and iron in shipwrecks cause conservation concerns, Chem. Soc. Rev. 35 (2006) 399–415.
[8] G. Almkvist, I. Persson, Extraction of iron compounds from wood from the Vasa, Holzforschung 60 (2006).
[9] J.W. Baty, C.L. Maitland, W. Minter, M.A. Hubbe, S.K. Jordan-Mowery, Deacidification for the conservation and preservation of paper-based works: a review, BioResources 5 (2010) 1955–2023.
[10] B. Reissland, Ink corrosion. Aqueous and non-aqueous treatment of paper objects – state of the art, Restaurator 20 (1999) 167–180.
[11] J. Kolar, M. Strlič, M. Budnar, J. Malesič, V.S. Šelih, J. Simčič, Stabilisation of corrosive iron gall inks, Acta Chim. Slov. 50 (2003) 763–770.
[12] J. Kolar, A. Možir, A. Balažic, M. Strlič, G. Ceres, V. Conte, et al., New antioxidants for treatment of transition metal containing inks and pigments, Restaurator 29 (2008) 184–198.
[13] U. Henniges, R. Reibke, G. Banik, E. Huhsmann, U. Hähner, T. Prohaska, et al., Iron gall ink-induced corrosion of cellulose: aging, degradation and stabilization. Part 2: application on historic sample material, Cellulose 15 (2008) 861–870.
[14] A. Potthast, U. Henniges, G. Banik, Iron gall ink-induced corrosion of cellulose: aging, degradation and stabilization. Part 1: model paper studies, Cellulose 15 (2008) 849–859.
[15] G. Poggi, R. Giorgi, N. Toccafondi, V. Katzur, P. Baglioni, Hydroxide nanoparticles for deacidification and concomitant inhibition of iron-gall ink corrosion of paper, Langmuir 26 (2010) 19084–19090.
[16] G. Poggi, P. Baglioni, R. Giorgi, Alkaline earth hydroxide nanoparticles for the inhibition of metal gall ink corrosion, Restaurator 32 (2011) 247–273.
[17] M. Strlič, J. Kolar, V.S. Šelih, D. Kocar, B. Pihlar, A comparative study of several transition metals in Fenton-like reaction system at circum-neutral, Acta Chim. Slov. 50 (2003) 619–632.
[18] M. Ambrosi, L. Dei, R. Giorgi, C. Neto, P. Baglioni, Colloidal particles of $Ca(OH)_2$: properties and applications to restoration of frescoes, Langmuir 17 (2001) 4251–4255.
[19] R. Giorgi, L. Dei, M. Ceccato, C. Schettino, P. Baglioni, Nanotechnologies for conservation of cultural heritage: paper and canvas deacidification, Langmuir 18 (2002) 8198–8203.
[20] R. Giorgi, D. Chelazzi, P. Baglioni, Nanoparticles of calcium hydroxide for wood conservation. The deacidification of the Vasa warship, Langmuir 21 (2005) 10743–10748.
[21] R. Giorgi, D. Chelazzi, P. Baglioni, Conservation of acid waterlogged shipwrecks: nanotechnologies for de-acidification, Appl. Phys. A: Mater. Sci. Process. 83 (2006) 567–571.

[22] D. Chelazzi, R. Giorgi, P. Baglioni, Nanotechnology for Vasa wood deacidification, Macromol. Symp. 238 (2006) 30–36.
[23] S. Sequeira, C. Casanova, E.J. Cabrita, Deacidification of paper using dispersions of $Ca(OH)_2$ nanoparticles in isopropanol. Study of efficiency, J. Cult. Herit. 7 (2006) 264–272.
[24] E. Stefanis, C. Panayiotou, Protection of lignocellulosic and cellulosic paper by deacidification with dispersions of micro- and nano-particles of $Ca(OH)_2$ and $Mg(OH)_2$ in alcohols, Restaurator 28 (2007) 185–200.
[25] E. Stefanis, C. Panayiotou, Deacidification of documents containing iron gall ink with dispersions of $Ca(OH)_2$ and $Mg(OH)_2$ nanoparticles, Restaurator 31 (2010) 19–40.
[26] R. Giorgi, M. Ambrosi, N. Toccafondi, P. Baglioni, Nanoparticles for cultural heritage conservation: calcium and barium hydroxide nanoparticles for wall painting consolidation, Chem. – Eur. J. 16 (2010) 9374–9382.
[27] D. Chelazzi, G. Poggi, Y. Jaidar, N. Toccafondi, R. Giorgi, P. Baglioni, Hydroxide nanoparticles for cultural heritage: consolidation and protection of wall paintings and carbonate materials, J. Colloid Interface Sci. 392 (2013) 42–49.
[28] G. Madras, B.J. McCoy, Ostwald ripening with size-dependent rates: similarity and power-law solutions, J. Chem. Phys. 117 (2002) 8042–8049.
[29] J.A. Marqusee, J. Ross, Kinetics of phase transitions: theory of Ostwald ripening, J. Chem. Phys. 79 (1983) 373–378.
[30] T. Sugimoto, General kinetics of Ostwald ripening of precipitates, J. Colloid Interface Sci. 63 (1978) 16–26.
[31] G. Oskam, Z. Hu, R.L. Penn, N. Pesika, P.C. Searson, Coarsening of metal oxide nanoparticles, Phys. Rev. E 66 (2002) 011403.
[32] T. Sugimoto, Kinetics of reaction-controlled Ostwald ripening of precipitates in the steady state, J. Colloid Interface Sci. 63 (1978) 369–377.
[33] M. Inoue, Solvothermal synthesis of metal oxides, in: S. Somiya (Ed.), Handb. Adv. Ceram., second ed., Academic Press, Oxford, 2013, pp. 927–948.
[34] H. Zhou, H. Wang, K. Zheng, Z. Gu, Z. Wu, X. Tian, Aluminum-doped zinc oxide nanoparticles with tunable near-infrared absorption/reflectance by a simple solvothermal process, RSC Adv. 4 (2014) 42758–42763.
[35] T.-D. Nguyen, From formation mechanisms to synthetic methods toward shape-controlled oxide nanoparticles, Nanoscale 5 (2013) 9455–9482.
[36] P.A. Hassan, S. Rana, G. Verma, Making sense of Brownian motion: colloid characterization by dynamic light scattering, Langmuir 31 (2015) 3–12.
[37] W.D. Pyrz, D.J. Buttrey, Particle size determination using TEM: a discussion of image acquisition and analysis for the novice microscopist, Langmuir 24 (2008) 11350–11360.
[38] T.A. Ring, Fundamentals of Ceramic Powder Processing and Synthesis, Academic Press, San Diego, 1997.
[39] M. Strlič, J. Kolar, M. Zigon, B. Pihlar, Evaluation of size-exclusion chromatography and viscometry for the determination of molecular masses of oxidised cellulose, J. Chromatogr. A 805 (1998) 93–99.
[40] L. Santucci, M.P. Zappalà, Cellulose viscometric oxidometry, Restaurator 22 (2001) 51–65.
[41] G. Banik, Mass deacidification technology in Germany and its quality control, Restaurator 26 (2005) 63–75.
[42] G. Wypych, Handbook of Solvents, ChemTec, Toronto, New York, 2001.
[43] J. Catalán, C. Díaz, A generalized solvent acidity scale: the solvatochromism of o-tert-butylstilbazolium betaine dye and its homomorph o,o′-di-tert-butylstilbazolium betaine dye, Liebigs Ann. 1997 (1997) 1941–1949.
[44] M.J. Kamlet, R.W. Taft, The solvatochromic comparison method. I. The beta-scale of solvent hydrogen-bond acceptor (HBA) basicities, J. Am. Chem. Soc. 98 (1976) 377–383.
[45] X. Liu, X. Piao, Y. Wang, S. Zhu, Calcium ethoxide as a solid base catalyst for the transesterification of soybean oil to biodiesel, Energy Fuels 22 (2008) 1313–1317.
[46] Portlandite XRD – RRUFF Database (ID: RO70210.1), <http://rruff.info/portlandite/display=default/> (accessed 05/17/13, n.d.).
[47] D. Fengel, G. Wegener, Wood: Chemistry, Ultrastructure, Reactions, Walter De Gruyter, Berlin and New York, 1984.
[48] D.I. Donato, G. Lazzara, S. Milioto, Thermogravimetric analysis, J. Therm. Anal. Calorim. 101 (2010) 1085–1091.
[49] G. Cavallaro, D. Donato, G. Lazzara, S. Milioto, Determining the selective impregnation of waterlogged archaeological woods with poly(ethylene) glycols mixtures by differential scanning calorimetry, J. Therm. Anal. Calorim. 109 (2012) 1–7.
[50] E.J. Schofield, R. Sarangi, A. Mehta, A.M. Jones, F.J.W. Mosselmans, A.V. Chadwick, Nanoparticle de-acidification of the Mary Rose, Mater. Today 14 (2011) 354–358.
[51] A.V. Chadwick, E.J. Schofield, A.M. Jones, G. Cibin, J.F.W. Mosselmans, Ionic nanoparticles in heritage conservation; treatments for the Mary Rose timbers, Solid State Ionics 225 (2012) 742–746.
[52] M. Sandström, Y. Fors, I. Persson, The Vasa's new battle – sulphur, acid and iron, Stock. VasaMuseet – Vasastudier 19 (2003).